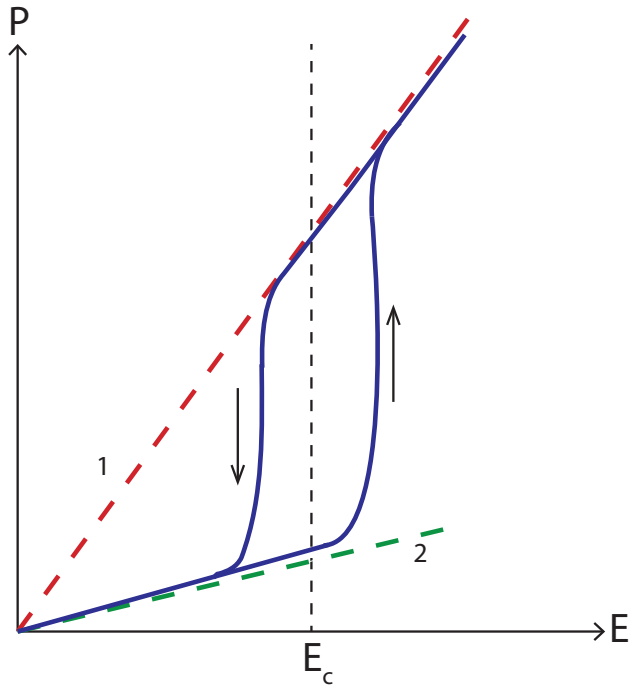

Supplementary Figure S1. Double hysteresis loops predicted by the two-instability model for antiferroelectricity. Schematic $P-E$ dependences: obtained from relationship (S9) - red dashed line 1, obtained from the set of equations (S6) and (S5) - green dashed curve 2, the total $P-E$ dependence taking into account the phase coexistence in the vicinity the first-order phase transition - solid blue curve.

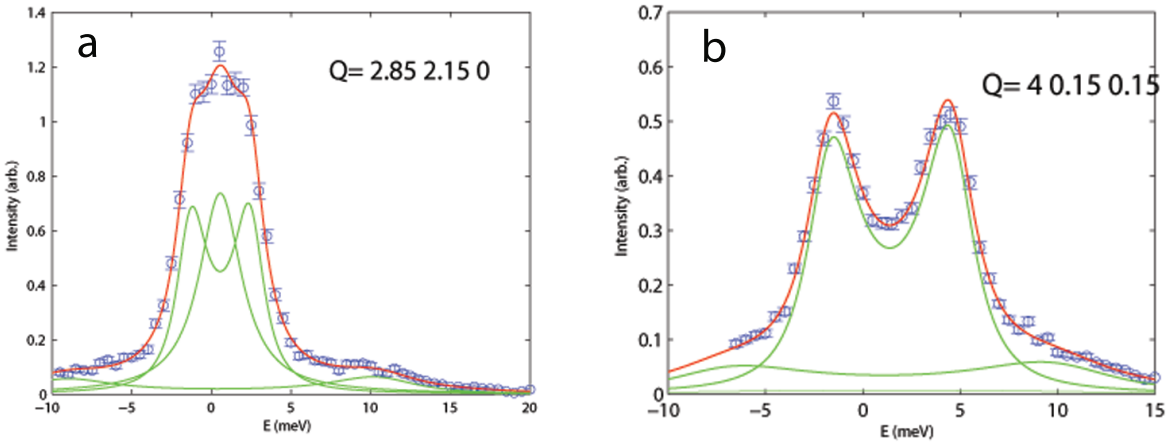

Supplementary Figure S2. Experimentally measured IXS spectra at T=780 K (E – Energy transfer in meV) for the reduced scattered wavevectors **q**=(0.15 0.15 0); a – in-plane polarized (along $[1\bar{1}0]$) and b – out-of-plane polarized (along [001]). The wavevectors are measured in the units of the reciprocal cubic lattice constant $a^* = 2\pi/a$.

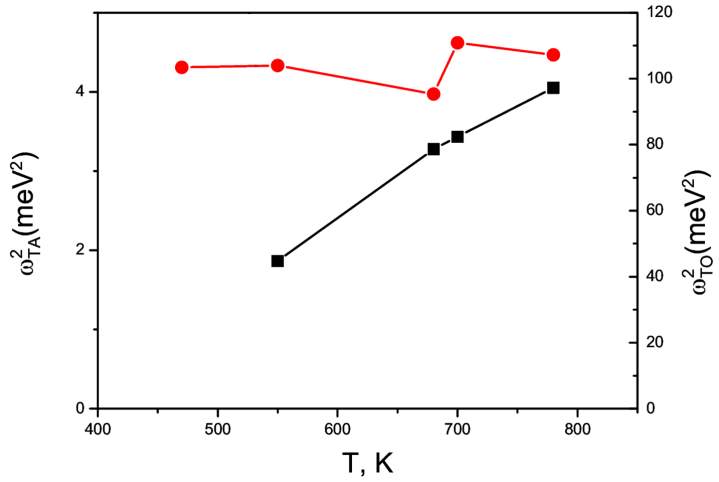

Supplementary Figure S3. Temperature dependences of the enegy squared of the TA (black squares) and TO (red circles) phonons in the cubic phase at **q**=(0.15 0.15 0). **q** is measured in the units of the reciprocal cubic lattice constant $a^* = 2\pi/a$.

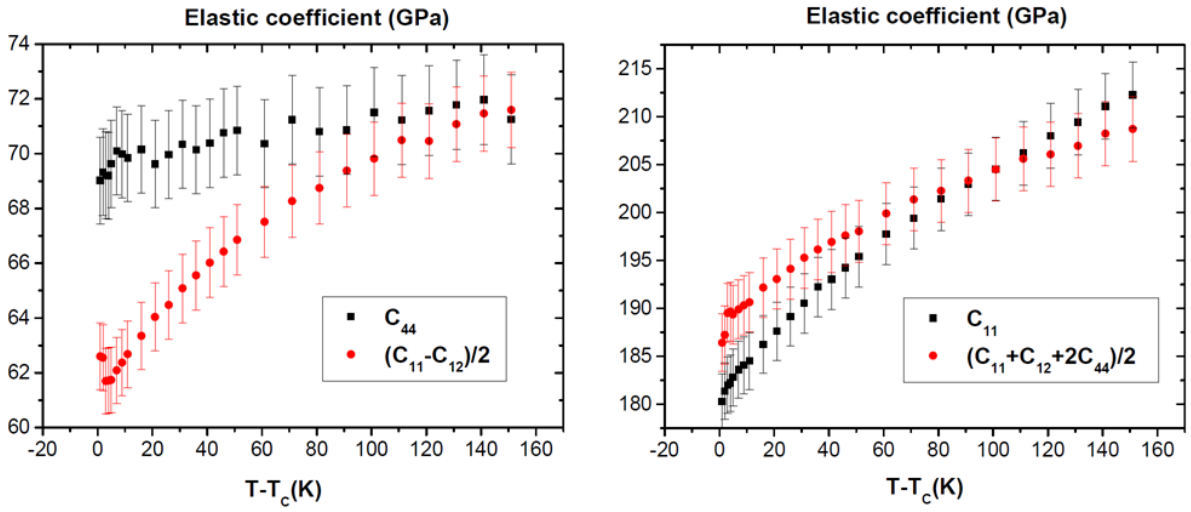

Supplementary Figure S4. Temperature dependence of elastic coefficients of PZ single crystals above the antiferroelectric phase transition determined from the Brillouin light scattering data

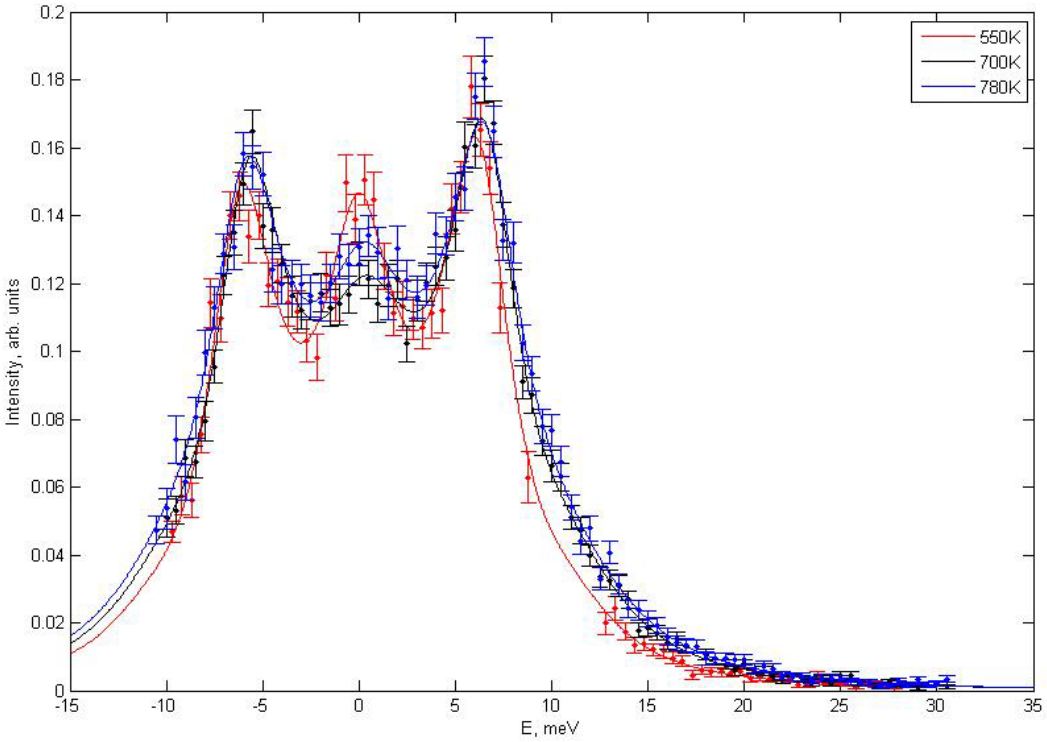

Supplementary Figure S5. Experimentally measured IXS spectra at the R-point (**Q**=(3.5 0.5 0.5)) at several temperatures. **Q** is measured in the units of the reciprocal cubic lattice constant $a^* = 2\pi/a$.

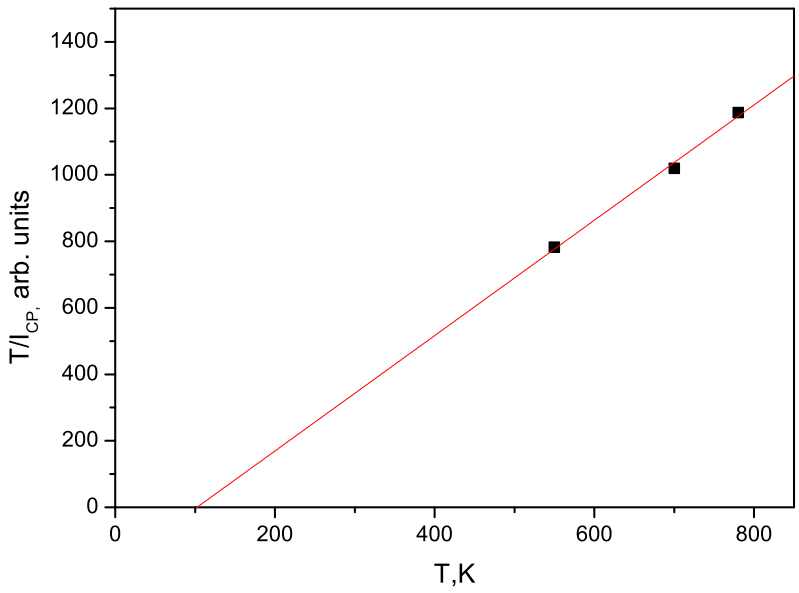

Supplementary Figure S6. $T/I_{CP}(T)$ dependence, where I_{CP} - integrated intensity of the central line at R-point (**Q**=(3.5 0.5 0.5)). **Q** is measured in the units of the reciprocal cubic lattice constant $a^* = 2\pi/a$.

SUPPLEMENTARY NOTE 1: TWO-INSTABILITY MODEL FOR ANTIFERROELECTRICITY

In the main text, the characteristic dielectric anomaly accompanying an antiferroelectric phase transition has been explained using the two-instability model. Another characteristic feature of such transitions is the observation of double polarization-field ($P-E$) hysteresis loops. Here we demonstrate how the double hysteresis loops can be explained using the same model. First, we specify expansion (1) from the main text so that it explicitly describes a first order phase transition with respect to the order parameter ξ at T_A:

$$F(P,\xi) = \frac{1}{2}A(T-T_0)P^2 + \frac{1}{2}\delta_{\mathrm{P}}P^2\xi^2 + \frac{1}{2}\alpha(T-T_0^{\mathrm{str}})\xi^2 + \frac{1}{4}\beta\xi^4 + \frac{1}{6}\gamma\xi^6 \tag{S1}$$

where $\beta < 0$ and $\gamma > 0$. From the theory of the first order phase transition[36] we derive the equation of state for ξ

$$\alpha(T-T_0^{\mathrm{str}}) + \beta\xi^2 + \gamma\xi^4 = 0 \tag{S2}$$

and

$$\xi_0^2 = -\frac{3\beta}{4\gamma} \tag{S3}$$

$$\alpha(T_{\mathrm{A}}-T_0^{\mathrm{str}}) = \frac{3\beta^2}{16\gamma} \tag{S4}$$

where ξ_0 is the spontaneous value of the order parameter ξ at the transition temperature (i.e. at $T = T_{\mathrm{A}}$). The application of a dc electric field E induces a polarization P, modifying the equation of state, (S2), to the following:

$$\delta_{\mathrm{P}}P^2 + \alpha(T-T_0^{\mathrm{str}}) + \beta\xi^2 + \gamma\xi^4 = 0 \tag{S5}$$

where P satisfies the equation of state $\partial F/\partial P = E$ which can be rewritten as

$$[A(T-T_0) + \delta_{\mathrm{P}}\xi^2]P = E. \tag{S6}$$

Equation (S5) implies a field-induced lowering of the transition temperature (owing to the positive sign of δ_{P}). This means that at a temperature T in the antiferroelectric phase, the applications of a large enough electric field could possibly shift the transition temperature down to this temperature. Thus, at a fixed temperature, one can speak about a field-induced first-order phase transition with respect to the order parameter ξ. In general, this phase transition is accompanied with a sudden change in the dielectric permittivity. Since this

jump occurs at a finite value of the electric field, when considered along with the first order phase transition described above, it implies double hysteresis loops on the $P-E$ curve.

Alternatively, a more detailed description of this effect is as follows. Combining equations (S4) and (S5) one finds the value of the field-induced polarization, $P_{\rm C}$, corresponding to field-induced shift of the transition temperature $T_{\rm A}$ down to temperature T:

$$P_{\rm C} = \sqrt{\frac{\alpha(T_{\rm A}-T)}{\delta_{\rm P}}}. \tag{S7}$$

The critical field for the field-induced phase transition, $E_{\rm C}$, following from Eqs.(S6), (S7), and (S3), is given by

$$E_{\rm C} = \sqrt{\frac{\alpha(T_{\rm A}-T)}{\delta_{\rm P}}}\left[A(T-T_0) - \delta_{\rm P}\frac{3\beta}{4\gamma}\right]. \tag{S8}$$

Thus, at $T < T_{\rm A}$ in the antiferroelectric phase, the state with $\xi \neq 0$ is energetically favorable for $E < E_{\rm C}$. Conversely, the state with $\xi = 0$ is favorable for $E > E_{\rm C}$, . Therefore, neglecting a possible coexistence of phases in the vicinity the first-order phase transition, for $E > E_{\rm C}$ the dielectric response of the system is controlled by the relationship

$$A(T-T_0)P = E \tag{S9}$$

while for $E < E_{\rm C}$ it is controlled by the set of equations (S6) and (S5). Using these equations, if P is plotted as a function of E while taking into account the phase coexistence around $E_{\rm C}$, one finds that this dependence clearly shows "antiferroelectric" hysteresis loops as shown schematically in Supplementary Fig. S1.

The above discussion elucidates the true origin of the double hysteresis loops observed below the antiferroelectric phase transition. These loops correspond to the field-induced first order phase transition between the low-symmetry and high-symmetry phases with respect to the structural order parameter ξ. Hence, we believe that there is no ground to use the term "field induced ferroelectric state" for the state of the system at $E > E_{\rm C}$.

One should mention that formally, the model discussed will still exhibit the double hysteresis loops if the ferroelectric instability is absent[37], just a structural ("non-ferroelectric") first order phase is needed. However, in reality, without the ferroelectric instability providing the enhanced values of dielectric susceptibility, the critical field for the field-induced phase transition $E_{\rm C}$ will be unrealistically high.

The two-instability model also allows for an antiferroelectric to ferroelectric phase transition given a small chemical modification or the application of hydrostatic pressure. Indeed, in view of the small difference between the temperatures T_0 and $T_{\rm A}$, which is the key element of the model, the aforementioned factors may swap the relative positions of these temperatures. In this case the ferroelectric phase transition will take place first on cooling. Such a scenario corroborates with the appearance of ferroelectricity once PZ is slightly doped with Ti[38].

SUPPLEMENTARY NOTE 2: INELASTIC X-RAY SCATTING FOR THE Σ DIRECTION

Experimentally observed spectra are extremely anisotropic and depend on the polarization vectors as well. In the case of the excitations propagating in the [110] direction and polarized in the $[1\bar{1}0]$ direction (in-plane polarization), extremely low-lying TA phonon resonances were observed accompanied with a broad (broader than the resolution) central peak and weak TO phonon resonances (Supplementary Fig. S2a). The central peak can be identified with the central mode reported by Ostapchuk et al[21].

In the case of the excitations propagating in the [110] direction and polarized in the [001] direction (out-of-plane polarization), well-resolved TA phonon resonances and weak TO phonon resonances were observed (Supplementary Fig. S2b). The rather broad phonon resonance at about 10 meV can be identified with the TO mode. There is very subtle if any temperature dependence for this phonon (Supplementary Fig. S3).

SUPPLEMENTARY NOTE 3: ELASTIC CONSTANTS FROM BRILLOUIN LIGHT SCATTERING MEASUREMENTS

A conventional tandem multi-pass Fabry-Perot interferometer was used to measure the Brillouin spectrum in a narrow (13 GHz) frequency range by using a free spectra range of 15 GHz. The PZ sample was placed in a cryostat (FTIR 600, Linkam) which was set up vertically for forward, symmetric scattering experiment. A solid state laser (Excelsior 532-300, SpectraPhysics) at a wavelength of 532 nm was used as an excitation source. The details of the Brillouin spectrometer can be found elsewhere[39]. The temperature dependence of the elastic constants above the antiferroelectric phase transition determined from the Brillouin light scattering data are shown in Supplementary Fig. S4.

SUPPLEMENTARY NOTE 4: CENTRAL PEAK

In this section we discuss the relationship between the central peak that is present in our IXS spectra and the soft TO mode that is the driving force of the transition. The understanding of this relationship is important for the assessment of our main result, so we describe it here in greater detail. The fact that the development of the zone-center ferroelectric instability in PZ is connected mostly with quasielastic part of the spectrum is evident from IR data of Ostapchuk et al.[21] Our IXS spectra demonstrate the same - there is a critical temperature dependence of the central peak. This allows us to tentatively connect the central peak with the soft mode.

Howewer we note that this does not necessarily mean that the soft mode in PZ can be viewed just as an overdamped harmonic oscillator. As we mention in the main text - it is only a trace of the critical lattice softening process. In accord with the currently accepted approach, developed in the last 40 years and widely discussed in the literature[23,24,41,42], the connection between the soft mode and the central peak near a structural transition can be rationalized as follows[42].

In the quasiharmonic approximation one can write the following expression for the spectral correlation function A_λ, where λ is a composite index including the reduced wavevector and mode "number" :

$$A_\lambda(\omega) = \frac{1}{\pi} Im \left[\Omega_\lambda^2 - \omega^2 + \Pi_\lambda^{an}(\omega)\right]^{-1} \tag{S10}$$

Here Ω_λ stands for undisturbed harmonic frequency and $\Pi_\lambda^{an}(\omega)$ stands for self-energy function.

$$\Pi_\lambda^{an}(\omega) = \Delta_\lambda^0 + i\omega\Gamma_\lambda^0, \tag{S11}$$

Δ_λ^0 and $\omega\Gamma_\lambda^0$ are frequency independent constants. This formula corresponds to the classical damped harmonic oscillator with a characteristic "quasiharmonic" frequency:

$$\omega_\infty^2 = \Omega^2 + \Delta^0, \tag{S12}$$

hereafter the index λ is omitted. The appearance of the central peak can be accounted for by introducing the frequency dependence of the parameters Δ and Γ, which is presented in

the form:

$$\Delta(\omega) = \Delta^0 - \delta^2 \left[\frac{\gamma^2}{\gamma^2 + \omega^2}\right] \tag{S13}$$

$$\Gamma(\omega) = \Gamma^0 + \delta^2 \left[\frac{\gamma^2}{\gamma^2 + \omega^2}\right] \tag{S14}$$

The introduction of the such frequency dependences results in a 2-component response. There is a double-peak damped harmonic oscillator component:

$$S_{\mathrm{DHO}}(\omega) = \frac{\Gamma^0}{(\omega_\infty^2 - \omega^2)^2 + (\omega\Gamma^0)^2} \tag{S15}$$

and a central peak component

$$S_{\mathrm{CP}}(\omega) = \left(\frac{\delta^2}{\omega_0^2 \omega_\infty^2}\right) \frac{\gamma'}{\omega^2 + \gamma'^2}. \tag{S16}$$

Here

$$\omega_0^2 = \omega_\infty^2 - \delta^2 \tag{S17}$$

and $\gamma' = \gamma(\omega_0/\omega_\infty)^2$.

The exact microscopic origin behind this formalism is not yet fully known, but there were collected numerous evidences that it could be considered as a phenomenological starting point for the analysis of real examples. It is important to note that in this framework the quasiharmonic frequency ω_∞ of the TO mode can be substantially renormalized (see Eq. (S12)) with respect to the ω_0 frequency, whose temperature dependence defines the critical process. Due to that, in the experiment, one may observe nearly temperature-independent phonon resonances (as it is the case for PZ) that are accompanied by a strongly temperature dependent central peak manifesting the critical lattice softening (as it is the case for PZ). Nevertheless the information on the true ω_0 frequency can indeed be reconstructed in the mentioned framework by the analysis of the central peak integral intensity, which is done in this work. Tentatively we associate the observed TO phonon resonances and the central peak with the renormalized Last-type TO mode and the rattling of Pb ions in the oxygen cage.

SUPPLEMENTARY NOTE 5: DETERMINATION OF THE R-POINT OXYGEN MODE SOFTENING

In this section we demonstrate the capability of IXS to quantitatively characterize the R-point oxygen mode softening despite the presence of the much heavier lead ions. In accord with the main message of the paper we show that there is no critical softening at the R-point.

In the harmonic approximation the dynamical structure factor for one-phonon scattering can be presented as[40]

$$S(\mathbf{Q},\omega) = \sum_j \langle n(\omega) + \frac{1}{2} \pm \frac{1}{2} \rangle \frac{1}{\omega_j(q)} F_{jn}(\mathbf{Q}) \delta(\omega \pm \omega_j(\mathbf{q})), \tag{S18}$$

where ω_j is the frequency of the j-th mode, $n(\omega)$ - the Bose factor and $F_{in}(\mathbf{Q})$ - the inelastic structure factor. The latter is given by a sum over the atoms in the unit cell

$$F_{jn}(\mathbf{Q}) = \left| \sum_a \frac{f_a(\mathbf{Q})}{\sqrt{M_a}} [\mathbf{e}_a^j(\mathbf{q}) \cdot \mathbf{Q}] \exp(i\mathbf{Q} \cdot \mathbf{r}_a) \exp(-w_a) \right|^2 . \tag{S19}$$

Here M_a represent masses of the ions, $f_a(\mathbf{Q})$ - the atomic scattering form factors, $\mathbf{e}_a^j(\mathbf{q})$ - the mode eigenvector, $\mathbf{r}_a$ - positions of the atoms in the unit cell and $\exp(-w_a)$ - the Debye-Waller factors, the suffix a enumerates the atoms in the unit cell. To obtain an estimate for possible relative intensities of scattering due to vibrations of heavy ions (soft mode) and light ions (oxygen mode) we roughly evaluate the contributions to the inelastic structure factor (S19) due to lead and oxygen atoms. For simplicity we neglect the difference in the Debye-Waller factors of the elements and use the approximation $f_a(Q) \approx f_a(0) = Z_a$ (where Z_a is the number of the element in the periodic table), which is reasonable for not too large Q. Let us obtain in this approximation the estimates for the largest possible contributions of these elements to the inelastic structure factors. In this case, the order of magnitude of the leading term in (S19) for the lead for $\mathbf{Q} = (3\ 2\ 0)$ will be $(\frac{Z_{\mathrm{Pb}}}{\sqrt{M_{\mathrm{Pb}}}} * Q)^2 = 422.28$ (with $Z_{\mathrm{Pb}} = 82$ and $M_{\mathrm{Pb}} = 207$) while for the oxygen at $\mathbf{Q} = (3.5\ 0.5\ 0.5)$ $(\frac{Z_{\mathrm{O}}}{\sqrt{M_{\mathrm{O}}}} * Q)^2 = 51$ (with $Z_{\mathrm{O}} = 8$ and $M_{\mathrm{O}} = 16$). From these estimates we can conclude that the scattering intensities of a lead containing mode and of a purely oxygen one, once these are of comparable frequencies, should differ less than one order of magnitude.

Indeed our measurements at the mentioned R-point give distinct spectra containing well-resolved phonon resonances as well as the central peak, which we can tentatively identify with the overdamped R_{25} mode (Supplementary Fig. S5). In contrast with the temperature

independent phonon resonances, the central peak demonstrates a traceable evolution with temperature. To quantify the evolution of the corresponding mode frequency we employed the fact that at high temperatures the temperature-normalized integral central peak intensity I_{CP}/T is proportional to the generalized static susceptibility. The temperature evolution of T/I_{CP} is presented in Supplementary Fig. S6.

Apparently, the softening of the R_{25} mode does not correspond to any critical process with characteristic temperature close to the transition temperature (503 K). The extrapolation of the temperature trend of T/I_{CP} gives the critical temperature about 100 K.

We can also provide an estimate of the absolute value for the R-point 'unperturbed' phonon frequency. It is the smallness of this value, which gives us the information about the potential instability of the crystal with respect to the relevant phase transformation. In view of the presence of the central peak, this frequency differs from that of the phonon resonance (Supplementary Fig. S5), as it is explained Supplementary Note 4. We will based our analysis on the framework described in this section. We assume that the normal phonon resonances and the central peak at R-point are both related to the same mode with 'unperturbed' frequency ω_0. The latter is connected with the frequency ω_∞, at which the phonon resonances are observed by Eq. (S17), where the parameter δ can be determined through the relationship[42]

$$\frac{I_{\mathrm{CP}}}{I_{\mathrm{Total}}} = \frac{\delta^2}{\omega_\infty^2}. \tag{S20}$$

Here I_{CP} and I_{Total} are integral intensities for the central peak and for the whole spectrum, respectively. Relationships (S17) and (S20) imply $\omega_0^2 = \omega_\infty^2(1 - I_{\mathrm{CP}}/I_{\mathrm{Total}})$. At 780 K from our experimental data the ratio $\frac{I_{\mathrm{CP}}}{I_{\mathrm{Total}}} = 0.72 \pm 0.03$ and the energy of phonon resonance $\omega_\infty = 6.6 \pm 0.3$ meV. This gives the 'unperturbed' mode frequency $\omega_0 = 3.5 \pm 0.35$ meV. At 550 K the result is the same to within the error bars.

SUPPLEMENTARY NOTE 6: DIFFUSE SCATTERING MODELING

We considered that the diffuse scattering originates from the lowest-energy phonon modes. The observed central peak was also considered as an optic mode, overdamped in agreement with Ref. 21. The calculation and analysis of corresponding lattice dynamics is simplified assuming the limit of long wavelengths and neglecting high-energy optic modes that are irrelevant here[27,28]. The resulting simplified Hamiltonian takes into account only 5 modes: 3 acoustic modes (2TA+LA) and 2 lowest-energy transverse optic modes (2TO). It reads[27,28]:

$$\mathcal{H}^{(5)} = \frac{1}{2}\sum_{q}\left[\dot{\mathbf{u}}_{-q}\dot{\mathbf{u}}_{q} + \mathbf{u}_{-q}\hat{A}(q)\mathbf{u}_{q} + \dot{\mathbf{x}}_{-q}\dot{\mathbf{x}}_{q} + \omega_0^2\mathbf{x}_{-q}\mathbf{x}_{q} + \mathbf{x}_{-q}\hat{S}(q)\mathbf{x}_{q} + 2\mathbf{u}_{-q}\hat{V}(q)\mathbf{x}_{q}\right] \quad \text{(S21)}$$

where u_1, u_2, u_3 and x_1, x_2 are the normal coordinates for the 2TA+LA and 2TO modes, in the reference frame $(X'Y'Z')$ with Z'-axis parallel to the reduced wavevector $\mathbf{q}$, respectively. The tensors $\hat{A}$, $\hat{S}$ and $\hat{V}$ describe the contribution of the short-range interactions and can be written as: $\hat{A} = q^2(A_l\hat{g}^l + A_t\hat{g}^t + A_a\hat{g}^a)$, $\hat{S} = q^2(S_t\hat{g}^t + S_a\hat{g}^a)$, $\hat{V} = q^2(V_t\hat{g}^t + V_a\hat{g}^a)$, where $\hat{g}^l_{\alpha\beta} = n_\alpha n_\beta$, $\hat{g}^t_{\alpha\beta} = \delta_{\alpha\beta} - n_\alpha n_\beta$, $\hat{g}^a_{\alpha\beta} = \gamma_{\alpha\beta\gamma\delta}n_\gamma n_\delta$. In these equations $\mathbf{n} = \mathbf{q}/q$, $\delta_{\alpha\beta}$ is the Kronecker delta, and $\gamma_{\alpha\beta\gamma\delta}$ is the tensor invariant with respect to the symmetry operations of the cubic point groups, which, in the cubic reference frame, is defined as $\gamma_{\alpha\beta\gamma\delta} = 1$ for $\alpha = \beta = \gamma = \delta$ and $\gamma_{\alpha\beta\gamma\delta} = 0$ otherwise. ω_0 is the energy of the Γ-point soft mode. The parameters of the matrices $\hat{A}$, $\hat{S}$, and $\hat{V}$ can be related to the coefficients of the free energy expansion (Eq.(4) of the main text): $A_l = (c_{12}+2c_{44})/\rho$, $A_t = c_{44}/\rho$, $A_a = (c_{11}-c_{12}-2c_{44})/\rho$, $S_t = g_{44}/\mu$, $S_a = (g_{11} - g_{12} - 2g_{44})/\mu$ $V_t = f_{44}/\sqrt{\mu\rho}$, $V_a = (f_{11} - f_{12} - 2f_{44})/\sqrt{\mu\rho}$ where ρ is the density and μ is the coefficient relating ω_0 with the inverse electric susceptibility α in the cubic phase: $\alpha = \mu\omega_0^2$. The relationships for V_t and V_a are approximate since they ignore the contribution of the dynamic flexoelectricity[16].

The standard solution to the dynamical problem with Hamiltonian (S21) gives the frequencies and eigenvectors of the renormalized lattice modes. The latter can be presented in the reference frame $(X'Y'Z')$ as the columns of the matrix

$$D = \begin{pmatrix} v^{(1)}_{TOX'} & v^{(2)}_{TOX'} & v^{(3)}_{TOX'} & v^{(4)}_{TOX'} & v^{(5)}_{TOX'} \\ v^{(1)}_{TOY'} & v^{(2)}_{TOY'} & v^{(3)}_{TOY'} & v^{(4)}_{TOY'} & v^{(5)}_{TOY'} \\ v^{(1)}_{TAX'} & v^{(2)}_{TAX'} & v^{(3)}_{TAX'} & v^{(4)}_{TAX'} & v^{(5)}_{TAX'} \\ v^{(1)}_{TAY'} & v^{(2)}_{TAY'} & v^{(3)}_{TAY'} & v^{(4)}_{TAY'} & v^{(5)}_{TAY'} \\ v^{(1)}_{LAZ'} & v^{(2)}_{LAZ'} & v^{(3)}_{LAZ'} & v^{(4)}_{LAZ'} & v^{(5)}_{LAZ'} \end{pmatrix}. \tag{S22}$$

The values $v^{(N)}_{S\alpha}$ describe the contributions of the unperturbed modes of the type S polarized along the axis α in the $(X'Y'Z')$ frame to the mode N in the coupled system. In the case of no mode coupling all $v^{N}_{S\alpha}$ are either 1 or 0. Eigenvectors in the original cubic crystallographic reference frame (XYZ) are restored by a known transformation, described by matrix $\mathbf{M}$ in Refs. 27 and 28.

In the frame (XYZ), the eigenvectors of (S21) will have 6 components ($w^{(i,1)}_1$, $w^{(i,1)}_2$, $w^{(i,1)}_3$, $w^{(i,2)}_1$, $w^{(i,2)}_2$, $w^{(i,2)}_3$) where $i = 1..5$ enumerates the eigenmodes and the upper scripts "1" and "2" specify the Cartesian components of the contributions from the unperturbed optic ("1") and acoustic ("2") modes. The intensity of integral diffuse scattering due to the considered modes is given by

$$I(\mathbf{Q}) \propto T \sum_{i=1}^{5} \sum_{l=1}^{2} \frac{1}{\omega_i^2(\mathbf{q})} |\mathbf{Q} \cdot \mathbf{w}^{(i,l)}(q)|^2. \tag{S23}$$

Here $\omega_i(\mathbf{q})$ are the frequencies of the renormalized phonon modes. The presented expression is similar to the usual one[24], but there are no phase factors $\exp i\mathbf{Q} \cdot \mathbf{r}_j$ while the $1/\sqrt{m_j}$ multipliers are to be included in the eigenvectors of unperturbed modes. Here $\mathbf{r}_j$ and m_j are the radius-vector and the mass of the j^{th} atom in the unit cell, respectively. We expect this formula to give the correct description of the shape of the DS around any reciprocal lattice point, while it cannot be used for the comparison of the intensity around different Bragg peaks.

The formalism described above contains eight parameters: A_l, A_t, A_a, S_t, S_a, V_t, V_a and ω_0. We simulate the 2D intensity map for 550 K. We use the value of $\omega_0 = 1.25$ meV at this temperature from the results of infrared measurements of Ostapchuk *et al.*[21]. The parameters controlling the dispersion of non-coupled acoustic branches can be recalculated on the basis of elastic constants c_{11}=194 GPa, c_{12}=61 GPa, c_{44}= 71 GPa determined from the data of our Brillouin scattering experiment, density ρ = 8 g/cm^3, and the cubic lattice constant a = 0.416 nm[5] of PZ: A_l = 2512 meV^2/rlu^2 A_t = 879 meV^2/rlu^2 A_a = -111 meV^2/rlu^2.

The parameters controlling the dispersion of the TO mode (S_t and S_a) cannot be directly determined by inelastic scattering because this mode is overdamped in PZ. In modeling we assume that the isotropic part of the TO dispersion is close to one in lead titanate[43] and use the value S_t=4330 meV^2/rlu^2. We restricted our consideration to isotropic coupling $V_a = 0$. The values of unperturbed TO anisotropy $S_a = -7100$ meV^2/rlu^2 and the isotropic coupling constant $V_t = 750$ meV^2/rlu^2 were determined by nonlinear least-squares fit of diffuse scattering distribution.

The magnitudes of the latter two values are similar to ones in other perovskites. In fact, the magnitude of coupling V_t is about two times smaller than for $PbTiO_3$[27]. The absolute value of the anisotropy parameter S_a is slightly smaller than in $KTaO_3$ and 2-3 times smaller than in $BaTiO_3$[27]. What makes the qualitative difference is the sign of S_a. Due to a positive S_a in $KTaO_3$ and $BaTiO_3$, the frequency for the out-of-plane polarized TA phonons is minimal for the $\{001\}$ planes, resulting in the observed shining diffuse planes. In $PbZrO_3$ the parameter S_a is negative and the frequency of the in-plane polarized TA phonons, propagating along $\langle 110 \rangle$ directions is minimal, as a result the shining diffuse rods are observed.

One can check that the spectral parameters used for simulation of the 2D intensity maps corroborate with the statement that PZ is not far from the incommensurate instability. The parameter $\Theta = (f_{11} - f_{12})/\sqrt{(c_{11} - c_{12})(g_{11} - g_{12})}$ can be readily expressed in terms of these parameters to find $\Theta = (2V_t + V_a)/\sqrt{(2A_t + A_a)(2S_t + S_a)} = 0.9$. Thus Θ is close to its critical value of 1. However, in view of neglecting the contribution of the dynamic flexoelectricity when linking $f's$ with $V's$, the value of Θ obtained should be taken with precaution.

SUPPLEMENTARY NOTE 7: INCOMMENSURATE INSTABILITY OF PEROVSKITES

The presence of the flexoelectric term (off-diagonal and linear in the spatial derivatives) in the free energy expansion (Eq.(4) of the main text) make the system potentially unstable with respect to spatial modulations of polarization and strain. The criterion for the appearance of such instability, formulated in terms of phonon eigenstates, was offered by Axe *et al*[14]. These authors also supposed that "the materials exhibiting such instability existed or would be found". For cubic (perovskite) materials, this criterion can be readily rewritten in terms of the c, g, and f tensors. For example, for the modulations along the $< 110 >$ directions, this criterion reads $f_{44}^2 < c_{44}g_{44}$ or $(f_{11} - f_{12})^2 < (c_{11} - c_{12})(g_{11} - g_{12})$. For typical perovskite ferroelectrics $BaTiO_3$ and $SrTiO_3$, using experimental data[27,44,45], these criteria can be substantialized as $|f_{44}| < 3.3\,\mathrm{V}$, $|f_{11} - f_{12}| < 7\,\mathrm{V}$ and $|f_{44}| < 2.4\,\mathrm{V}$, $|f_{11} - f_{12}| < 10\,\mathrm{V}$, respectively. According to order-of-magnitude estimates[15] and *ab initio* calculations in perovskites[46], the values of the components of the f tensor in perovskites are expected to be about $1 - 10$ V. Thus, we see that ferroelectric perovskites are not far from the modulation instability.

SUPPLEMENTARY NOTE 8: CHARACTERISTIC PATTERN OF THE LEAD DISPLACEMENTS

We show here that our model can reproduce the characteristic pattern of the lead displacements in PZ (Fig. 1c. of the main text). This pattern corresponds to the so-called Σ_3 normal mode[7] of the cubic structure exhibiting displacements[47]: $Zr_x = -Zr_y$, $Pb_x = -Pb_y$, $O_{Ix} = -O_{Iy}$, $O_{IIx} = -O_{IIIy}$, and $O_{IIIx} = -O_{IIy}$ (Fig. 1a of the main text). For the wave vector $\mathbf{k} = \mathbf{k}_\Sigma$, using Eqs. (5) and (8) from the main text, one can present the lead displacements in such mode in the form:

$$\mathbf{r}_{Pb} \propto \begin{pmatrix} -1 \\ 1 \\ 0 \end{pmatrix} \cos[\frac{\pi}{2a}(x+y) + \varphi] \tag{S24}$$

where x and y are the Cartesian coordinates in the cubic reference frame. One can readily check that the pattern (Fig. 1c. of the main text) is reproduced by Eq. (S24) for $\varphi = \pi/4, 3\pi/4, 5\pi/4, 7\pi/4$, describing the ground state of the system for $\beta_U > 0$. The four values of φ correspond to four translational domain states of one orientational domain state specified by the orientation of the modulation wave vector.

SUPPLEMENTARY REFERENCES

[36] Tagantsev, A. K., Cross, L. E., and Fousek, J. *Domains in ferroic crystals and thin films* (Springer, New York, 2010).

[37] Strukov, B. A., Levanyuk, A. P. *Ferroelectric Phenomena in Crystals* (Springer, Berlin, 1998).

[38] Jaffe, B., Cook, W. J., Jaffe, J. *Piesoelectric Ceramics* (Academic Press, London, 1971).

[39] Kim, J. H., Choi, J. -Y., Jeong, M. -S., Ko, J. -H., Ahart, M., Ko, Y. H., and Kim, K. J. Development of a high-pressure brillouin spectrometer and its application to an ethylene-vinyl acetate copolymer. *J. Korean, Phys. Soc.*, **60**, 1419–1423 (2012).

[40] Krisch, Michael *Inelastic X-Ray Scattering from Phonons,* Topics in Applied Physics, Volume 108 (2007).

[41] Riste, T., Samuelsen, E. J., Otnes, K., Feder J. Critical behaviour of $SrTiO_3$ near the 105 K phase transition. *Sol. St. Comm.* , **9**, 1455 - 1458 (1971).

[42] Axe J. D. and Shirane G. Inelastic-Neutron-Scattering Study of Acoustic Phonons in Nb_3Sn. *Phys. Rev. B.* , **8**, 1455 - 1458 (1973).

[43] Kempa, M., Hlinka, J., Kulda, J., Bourges, P., Kania, A., Petzelt, J. Lattice dynamics of cubic $PbTiO_3$ by inelastic neutron scattering, *Phase Transitions.*, **79**, 351-359 (2006).

[44] Eggenhoffner, R. Landolt-Bornstein - Numerical data and functional-relationships in science and technology, New series, Group 3, Crystal and solid-state physics, Vol 16, Subvol A, Oxides - Allmann,R, Pies,W, Weiss,A *Scientia*, **117**, 685-686 (1982).

[45] Tagantsev, Alexander K. and Courtens, Eric and Arzel, Ludovic Prediction of a low-temperature ferroelectric instability in antiphase domain boundaries of strontium titanate. *Phys. Rev. B*, **64**, 224107 (2001).

[46] Ponomareva, I. and Tagantsev, A. K. and Bellaiche, L. Finite-temperature flexoelectricity in ferroelectric thin films from first principles. *Phys. Rev. B*, **85**, 104101 (2012).

[47] Cowley, R. A. Lattice dynamics and phase transitions of strontium titanate. *Phys. Rev.*, **134**, A981–A997 (1964).